Biomaterials Science

ROYAL SOCIETY OF CHEMISTRY

PAPER

View Article Online
View Journal | View Issue

Cite this: *Biomater. Sci.*, 2025, **13**, 1010

The role of human intestinal mucus in the prevention of microplastic uptake and cell damage†

Ellen W. van Wijngaarden, [a,b] Sandra L. Arias,[c] Matthew Rhee,[c] Meredith N. Silberstein[a,b] and Ilana L. Brito*[b,c]

An increase in plastic waste and its release into the environment has led to health concerns over microplastics (MPs) in the environment. The intestinal mucosal layer is a key defense mechanism against ingested MPs, preventing the migration of particles to other parts of the body. MP migration through intestinal mucus is challenging to study due to difficulties in obtaining intact mucus layers for testing and numerous formulations, shapes, and sizes of microplastics. Previous studies have primarily used mucus from animals, hydrogel models, and mucus samples from other parts of the body as substitutes. This study examines how different MP compositions, sizes (40–500 nm), and surface functionalizations alter MP migration through human intestinal mucus; how the mucus layer protects cells from MP uptake, toxicity, and inflammation; and how the intestinal mucus prevents the migration of other environmental toxins *via* MP particles. The presence of a mucus layer also provides critical protection against cytotoxicity, reactive oxygen species production, and uptake for all particles tested, although certain functionalizations, such as streptavidin, are particularly harmful to cells with high toxicity and inflammation. Understanding the properties that assist of impede the diffusion of MPs through mucus is relevant to the overall bioaccumulation and health effects of MPs as well as drug delivery purposes.

Received 26th November 2024,
Accepted 8th January 2025

DOI: 10.1039/d4bm01574f

rsc.li/biomaterials-science

1 Introduction

Common types of MPs include polypropylene (PP), polyethylene (PE), polystyrene (PS), and polymethylmethacrylate (PMMA), used in cosmetics, textiles, and packaging, among other uses.[1] After disposal, plastics gradually break down into microplastics (MPs), defined by the National Oceanic and Atmospheric Administration (NOAA) as small plastic pieces <5 mm long.[2] These MPs often end up in the environment, in the soil, water, and air, and are ingested or inhaled.[3,4] According to the World Health Organization, the concentration of MPs in drinking water ranges between 0 and 10 000 particles per L with some studies reporting values as high as 2.40×10^5 particles per L for bottled water.[3,5] Although many particles pass through the human body, inhalation and ingestion of MPs can also lead to uptake and accumulation of particles in our bodies over time.[6]

Microplastics and nanoplastics (NPs) have gained increasing attention due to mounting evidence tying them to health issues. The gastrointestinal (GI) tract is the most likely site of exposure, due to ingestion of contaminated food,[7] and is therefore the site of many health effects. Direct impacts on the gut include reduced mucus secretion,[8] gut barrier dysfunction,[9] intestinal inflammation,[10,11] gut microbiota dysbiosis, metabolic disorders,[12] and altered iron transport.[7] Research has also shown that the particles are capable of migrating from the intestine to other organs[13] causing metabolic disorders,[8] liver inflammation,[12] neurotoxicity,[1] DNA damage,[1] and organ dysfunction.[1]

MPs can also facilitate the ingestion of other harmful chemicals.[14] The high surface area of MPs facilitates chemical attachment and absorption.[15] Some of these environmental pollutants can lead to additional health problems such as kidney disease, digestive problems, weakening of the bones, and nerve damage.[16] These include common water toxins such as heavy metals like cadmium (Cd), plastic additives, such as bisphenol A (BPA), food preservatives including butylated hydroxyanisole (BHA) and chemicals like dibutyl phthalate (DBP) used in paints and textiles.[17] The Environmental

[a]*Sibley School of Mechanical and Aerospace Engineering, Cornell University, Ithaca, NY 14850, USA*
[b]*Engineered Living Materials Institute, Cornell University, Ithaca, NY 14850, USA. E-mail: ibrito@cornell.edu*
[c]*Meinig School of Biomedical Engineering, Cornell University, Ithaca, NY 14853, USA*
† Electronic supplementary information (ESI) available. See DOI: https://doi.org/10.1039/d4bm01574f

Protection Agency (EPA) has set limits[16,18–20] for these chemicals as they have been shown to negatively affect aquatic life and human health due to bioaccumulation. However, additional work is needed to understand how MPs aggravate the health risks of other pollutants.

To prevent and mitigate these health impacts, the human intestine contains a mucosal layer that acts as a protective barrier, allowing the passage of certain substances while restricting others.[21,22] Mucus is a viscoelastic hydrogel network of long negatively charged bottlebrush-like glycoproteins.[6,23] Intestinal mucus is primarily comprised of the glycoprotein, MUC2.[24] The mucus is crosslinked, creating a mesh of both hydrophilic and hydrophobic domains with a mesh pore size ranging from ~100 nm to ~500 nm in the gut.[21,25] Some diseases, such as Crohn's disease and ulcerative colitis result in a compromised mucus layer.[26,27] The human body has several defense mechanisms against foreign substances such as an acidic stomach environment. However, previous studies have indicated that the stomach environment causes no significant alteration of the polymer surface of MPs, meaning that intestinal mucus is critical in preventing MP absorption.[28,29] While MPs have been linked to an array of health problems, it is unknown whether a dysfunctional mucus layer might put patients at a higher risk of MP exposure.

Understanding the chemical and biophysical properties that assist of impede the diffusion of MPs through mucus is relevant to the bioaccumulation of MPs needed to quantify health effects, and for the drug delivery applications using particles. However, previous work has several limitations.[30] Key studies have examined the effects of particle composition but are focused primarily on PS and PE particles. These are two of the most common microplastics which are often found in cosmetics, textiles, and paints, as well as have been identified in human stool samples, however, other compositions, such as polypropylene and acylates merit investigation.[7,8,12,31–37] Additional particle compositions, such as PMMA, used in this study lack extensive previous investigation but have been shown to be both an environmental and health concern.[38] This study examines particles including PMMA, and silica in addition to the PP, PS, and PE based on environmental abundance and accessibility. Silica, although not a plastic, was included due to high ingestion. Silica can comprise up to 2% weight in food according to the Food and Drug Administration guidelines.[39]

In addition to particle composition, other aspects of particles have been shown to alter the diffusion of microparticles through mucus or mucus hydrogel models, including particle size[6,40] and surface charge.[41,42] A challenge to studying the transport of MPs through mucus and uptake by human cells is the difficulty of obtaining intact human mucus samples. Mucus from colonoscopies is often damaged during bowel preparation.[43] Most of what is known about the MPs in intestinal mucus comes from alternate mucus models, such as porcine gastric mucus or airway mucus to replicate the stiff and stable properties of human intestinal mucus. In this study we use HT29-MTX cells that reach confluency and produce a robust mucus layer.[25,44] We leverage microrheology to track the migration of MPs through the mucus layer, while still attached to the cell monolayer, thereby preventing any damage to the mucosal structure. We examine factors affecting MP migration through human intestinal mucus using a broad range of particle sizes, surface functionalizations and compositions; determine the extent to which the mucus protects against cell cytotoxicity, ROS production, and uptake; and measure the protective effects of mucus against MPs combined with common environmental pollutants.

2 Experimental

2.1. Cell culture and exposure conditions

HT-29-MTX cells were grown as a monolayer in Dulbecco's Modified Eagle Medium (DMEM) containing 4.5 g L^{-1} glucose, L-glutamine, 10% fetal bovine serum (FBS), and without sodium pyruvate (Corning, Corning, NY) at 37 °C and a humidified atmosphere with 5% CO_2. The cells were grown until 21 days after initial seeding for a mature mucus layer. Cells were co-exposed to MPs and/or chemicals for 24 hours using a microplastic concentration of 1 mg ml^{-1} culture media.[7,45] The particle concentration and exposure time were selected to follow previous *in vitro* studies. The concentrations used for the chemicals followed EPA limits and were 5×10^{-6} mg ml^{-1}, 0.2 mg ml^{-1}, 0.0001 mg ml^{-1}, and 0.2 mg ml^{-1} for Cd, BHA, BPA, and DBP respectively.[16,18–20]

All particles were obtained from Abvigen (Newark, NJ) including functionalized MPs (Fig. 1). Dibutyl phthalate, cadmium chloride, butylated hydroxyanisole, and bisphenol A were all obtained from Sigma-Aldrich (St Louis, MO). To minimized particle agglomeration, the stock MP suspensions were sonicated for 20 minutes at a frequency of 40 kHz before being added to the culture media. For each test, cells treated with only cell culture media with no particles were included as negative controls. All tests were performed in triplicate.

2.2. Microrheology

Cells were cultured in 6-well plates (Corning) on 22 mm circular cover glasses (Thermo Fisher Scientific, Waltham, MA) for 21 days. When including an additional environmental pollutant, the chemical was added to the culture media 24 hours before testing. The particle of interest was added to the culture media at a concentration of 1 μl ml^{-1} and left to equilibrate for 15 minutes. The cover glass was then removed from the well and placed up-side-down in a 23 mm diameter fluorodish (World Precision Instruments, Sarasota, FL). The diffusion of particles through the mucus layer was imaged on an Elyra Super Resolution Microscope (Zeiss, Germany) using a 63×/1.4 oil objective and a sCMOS TV2 camera. A 500 frame time series was collected with a step of 0.05 s with at least 3 biological replicates and at different locations over the cell monolayer. The same imaging conditions were used for tracking particles in both mucus and phosphate buffered saline (PBS). Images were analyzed using ImageJ Trackmate software using the DoG detector and LAP tracker options.[46] Linking between frames

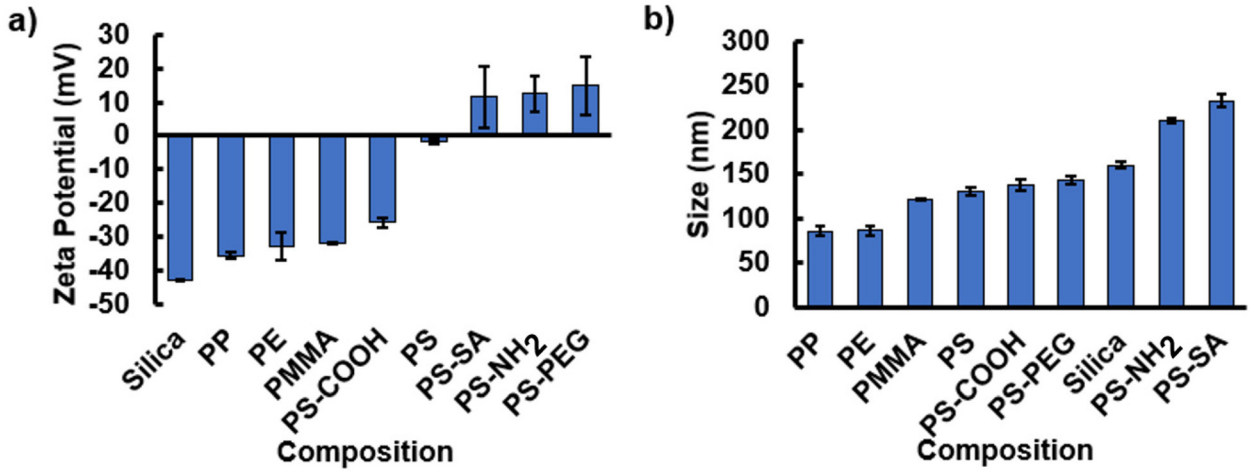

Fig. 1 (a) Zeta potential and (b) size distribution for MPs with various compositions tested in this study.

was set to 1 μm. Tracks were imported into Matlab (Mathworks, Natick, MA) for analysis using the msdanalyzer to determine mean squared displacements and diffusion coefficients for over 1000 tracks per sample group.

2.3. Surface charge and size

Zeta potential and size were measured using a Malvern Nano Zs Zetasizer (Malvern Pananalytical, Malvern, U.K.). Solutions were prepared in 2 ml tubes at a concentration of 0.1% weight to volume of deionized water given three hours to equilibrate before being transferred to polystyrene of zeta potential folded capillary cuvettes for measurement. All sample groups were tested in triplicate. A range of 40 nm to 500 nm particles were selected.

2.4. Cell viability assays

Cytotoxicity was tested using an MTT assay kit (Abcam, Boston, MA) which measures the reduction of 3-(4,5-dimenthythiazol-2yl)-2,5-diphenyltetrazolium bromide (MTT) to formazan salt due to the activity of cellular dehydrogenases and is an accepted assay for comparing cytotoxicity.[35] Confluent cell layers were grown in 96-well plates for 21 days. Cells part of the 'no mucus' group had the mucus layer flushed off by pipetting. Cells were then exposed to the relevant MPs and/or chemicals for 24 hours at the EPA limits for each chemical. Additional experiments were also conducted at chemical concentrations of 1 mg ml^{-1}, except for Cd, which had a concentration of 0.01 mg ml^{-1} due to its high cytotoxicity. After 24 hours, the media containing MPs and chemicals was removed and cells were washed with PBS two times before adding 50 μl of MTT reagent and 50 μl of serum free media were added to each well. The cells were incubated at 37 °C for 3 hours before adding 150 μl of MTT solvent to each well. The plates were wrapped in aluminum foil and placed on an orbital shaker for 15 minutes to dissolve the formazan crystals. The absorbance was then measured at 590 nm on a SpectraMax plate reader (SpectraMax, San Jose, Ca). The culture medium background was subtracted from the assay reading and the average of three readings was taken for each sample condition.

2.5. ROS

The production of reactive oxygen species (ROS) was measured using a dichlorodihydrofluorescein diacetate (DCFDA) kit (Abcam). Confluent cell layers were grown in 96-well plates. After 21 days, the mucus layer was removed *via* pipetting to cohesively delaminate and remove mucus from half of the wells. All cells were exposed to different MPs for 24 hours, using the same concentrations used for the MTT tests. Following exposure, the media containing MPs and chemicals was removed and 100 μl per well of 1× buffer was added. The 1× buffer was removed and 100 μl per well of diluted DCFDA solution was then added. Cells were incubated for 45 minutes at 37 °C in the dark. The DCFDA solution was removed following incubation and 100 μl per well of 1× buffer was added without phenol red. Tert-butyl hydroperoxide (TBHP) was added to 3 control wells for 3 hours as a positive control at a concentration of 50 μM according to the manufacturer recommendations. Following the 3 hour incubation, the plate was then measured immediately on a fluorescence plate reader at an excitation/emission of 485/535 nm. The control cell fluorescence was used to determine the ROS fold change and all values were corrected based on the number of cells determined through the MTT cytotoxicity assay (ROS fold change/(1-cytotoxicity/100%)) (section 2.4). All exposures were done in triplicate for each MP or chemical condition.

2.6. Flow cytometry

Flow cytometry was conducted to determine how cell uptake of MPs varied in the presence and absence of a mucus layer. Cells were grown in 24-well plates for 21 days. Half of the cells had the mucus layer removed before MPs were added at a concentration of 1 mg ml^{-1} for 24 hours. Following exposure, cells were washed three times with 0.5 ml PBS before being trypsi-

nized with 0.2 ml per well. Cells were washed and suspended in 0.5 ml per well DMEM + 10 T FBS per well before being transferred into a 2 ml tube. The tubes were centrifuged at 300*g* for 5 minutes and the supernatant was discarded. Cells were washed with 0.5 ml per well PBS before adding 1 μl of efluor 450 dye per 1 ml of cell solution. Samples were then vortexed immediately and incubated for 30 minutes at 2–8 °C, protected from light for live/dead staining. Cells were subsequently washed with PBS and centrifuged at 300*g* for 5 min. The supernatant was then discarded and the cell pellets were resuspended in 0.2 ml of 4% paraformaldehyde (PFA) in PBS for 10 minutes at room temperature for fixation. Cell suspensions were then centrifuged for 5 minutes at 300*g*, washed, and resuspended in PBS. Cells were centrifuged again to remove PBS and resuspend cells in FACS buffer (PBS and 10% FBS). Cells were filtered using a 40 μm FACS tube cell strainer (Thermo Fisher Scientific) and measured using an Attune *N* × *T* (Thermo Fisher Scientific) cytometer was used to measure fluorescence of the single cell suspension. Excitation and emission for each cell was measured at 488/507 nm, 405/450 nm and 651/660 nm.

2.7. Microscopy

Cells were grown in 8 well μ-sldies (Ibidi, Fitchburg, WI) and exposed to particles for 24 hours. Cells were stained with LysoTracker Deep Red in PBS (Thermo Fisher Scientific) at a concentration of 75 nM for 1 hour at 37 °C. Cells were covered with 0.2 ml per well. LysoTracker Deep Red stains lysosomes and late endosomes. A decrease in fluorescence of LysoTracker Deep Red provides an indication of cell damage. Cell layers were washed three times with PBS and fixed with 4% PFA in PBS for 10 minutes at room temperature. Following fixation, cells were washed three times with PBS. Hoechst 33342 (Thermo Fisher Scientific) was used to stain nuclei as a viability indicator at a dilution of 1 : 1000 in 1% BSA/PBS for 10 minutes at 37 °C protected from light. Cells were subsequently washed three times with PBS before aspirating media and imaging on a confocal multiphoton microscope using a 40× magnification water objective (Zeiss, Germany).

2.8. Statistical analysis

Two-tailed Student's *t*-test with equal variances were used to determine if statistically significant differences existed between groups. Correlation tests were conducted to determine trends between groups with multiple factors.

3 Results and discussion

3.1. Changes in MP diffusivity due to composition, surface charge, and size

We investigated the diffusivity of various particles in intact human intestinal mucus layers, still attached to the cell monolayer, using microrheology. We confirmed, through qPCR, that our intestinal cells express MUC2 at a higher level than either MUC5B or MUC5AC, matching healthy intestinal mucus (Fig. S1†).[47] The diffusivity value captures how key factors such as composition, surface functionalization, size, and surface charge affect particle migration through mucus. Theoretical predictions for the diffusivities of freely moving particles can be made by applying the Stokes–Einstein theory, which states that the diffusivity or diffusion coefficient is related to the temperature (T), solution viscosity (η), and particle radius (a) by the Boltzmann constant (k = 1.3807 × 10^{-23} J K^{-1}) and a factor of 1/6 π (eqn (1)).

$$D = \frac{kT}{6\pi\eta a}. \quad (1)$$

We verified that microrheology performed in PBS yields similar values to the theory as shown in Fig. S2.† The diffusivity values for particles moving in mucus would be expected to have lower diffusivity due to increased viscosity. Particle composition, charge, surface functionalization and non-homogeneous media contribute to deviations from the theoretical diffusivity values. Other models, such as the hopping model for the diffusion of nanoparticles in polymer matrices, proposed by Cai and Rubenstein, may provide better predictions but are impractical to apply due to the lack of characterization of intestinal mucin properties.[48,49]

Diffusivity was affected by both composition and size. We measured the diffusivity values for different particle compositions, as shown in Fig. 1a. Zeta potential values for the different compositions varied from −42.93 mV to 14.96 mV, as shown in Fig. 1a. Note that particle size also ranges somewhat due to additional surface functionalizations and manufacturer processing variation (Fig. 1b). The diffusivity values for various 100 nm particle compositions range from 0.63 $\mu m^2\ s^{-1}$ to 3.14 $\mu m^2\ s^{-1}$ (Fig. 1a). All diffusivity values for different compositions and surface functionalizations with the same theoretical size were statistically significantly different from one another (P-values < 0.0001) (Fig. S3†). Assuming a 50 μm thick mucus layer, the time to diffuse through the mucus would range from 13–63 hours for the differently composed particles, assuming the mucus is homogeneous and the particle sizes are uniform. The estimated thickness value is based on *in vivo* rodent studies of the inner colonic mucus layer.[50] The thickness of the human inner mucus layer is yet to be accurately measured and the mechanisms controlling mucus thickness are not yet understood.[50] Therefore, we have considered the current *in vivo* thickness data available for the inner colonic mucus layer that adheres to the cell layer as the mucus does in our model. The particles with the highest diffusivities include PS, PE, PS-PEG, and PS-COOH. The close to neutral charge of PS might contribute to its high diffusivity value. Carboxylic acid groups can cause dispersion of mucus aggregates slightly increasing the diffusivity of this group.[51] PEG is well known for being bioinert and acts to shield particles from mucus interactions, thereby increasing diffusivity.[52] The particles with the lowest diffusivity values are silica, PS-SA, and PS-NH_2. These particles were measured to be above the theoretical size of 100 nm. These functionalizations alter surface charge and

may also increase the interactions with mucus, hindering migration throughout the mucus layer. Previous studies also report that amine-functionalized particles diffuse more slowly than carboxylic acid particles, likely due to differences in charge.[53] Streptavidin is also known to bind with biotin which is critical for maintaining mucus surfaces.[54,55] A combination of composition, surface charge and surface functionalization results in each particle group having a statistically unique diffusivity value for the same manufacturer defined size (Fig. 2 and S3†).

The diffusivity values show a statistically strong trend with particle size and zeta potential. As expected, according to the Stokes–Einstein equation, decreasing particle radius increases diffusivity with a correlation coefficient, r, equal to −0.94, indicating a strong negative correlation between size and diffusivity ($|r|>0.5$) (Fig. 2b). The 500 nm particles did not diffuse through the mucus as these are larger than the mucus mesh size of approximately 214 nm.[25] In contrast, the 40 nm particles diffused easily through the mucus matrix. Fig. 2c shows a clear decrease in diffusivity approaching the mucus mesh size when comparing all the particles measured, with R^2 values of the PBS and mucus power law trendlines of 0.67 and 0.57 respectively, as previously reported. In contrast, Cobarrubia *et al.* reported an R^2 value of only 0.30 in a literature review of particle diffusivity related to particle size for various compositions in different mucus samples.[56] Additionally, we find that the same particles plotted according to zeta potential show a parabolic trend in both the PBS

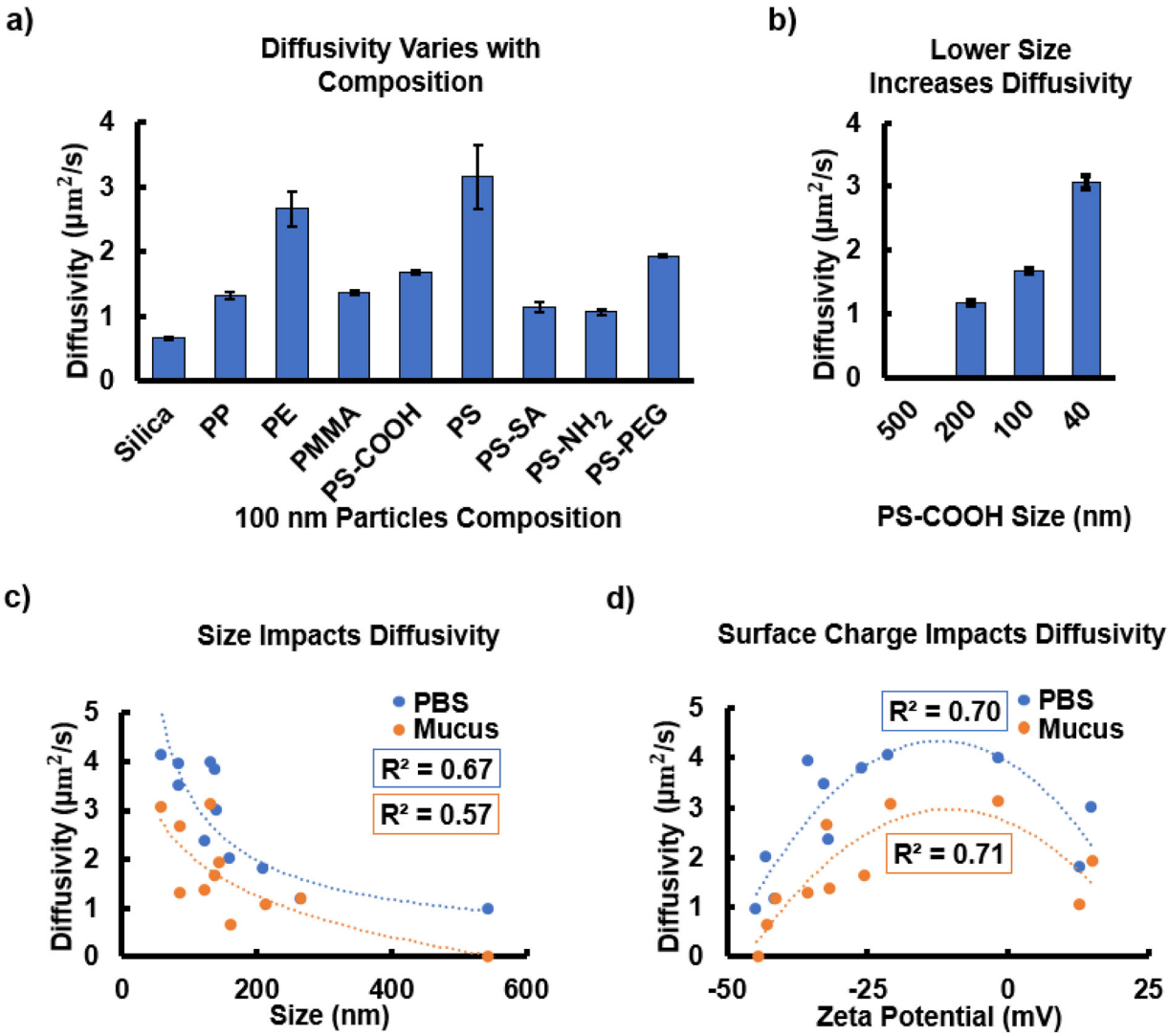

Fig. 2 Surface charge and particle size are key factors affecting particle migration. (a) Diffusivity of 100 nm particles with varied functionalization and composition within the mucus layer. All compositions are statistically significantly different from one another (p-value < 0.0001) (Fig. S3†). (b) Diffusivity for 500 nm, 200 nm, 100 nm, and 40 nm PS-COOH particles within the mucus layer. All sizes are statistically significantly different from one another (p-value < 0.0001). (c) Diffusivity shows a parabolic trend with zeta potential for particles suspended in PBS and within the mucus layer attached to cells. (d) Diffusivity decreases with increasing particle size with values well below the theoretical limits for diffusion for spherical particles based on thermodynamic forces opposed by only the drag of the fluid.

control (R^2 = 0.70) and the mucus (R^2 = 0.71) samples with neutral and slightly negative particles having the highest diffusivity values (Fig. 2d). Cobarrubia *et al.* reported an R^2 value of 0.67 in their review of particle diffusivity and zeta potential.[56] The mucus curve appears to be shifted downward in both plots, as expected, due to the higher viscosity.

3.2. Cellular uptake of particles with and without the mucosal barrier

We next asked whether mucus acts as a barrier to prevent the uptake of all types of particles. Decreased fluorescence of Hoechst 33342 and LysoTracker Deep Red in the absence of mucus compared to when a mucus layer was present, indicates decreased viability and membrane destabilization of the acidic vacuolar compartment, aligning with previous work by Visalli *et al.* (Fig. 3a, S4–S7†).[7] The mechanism of cell death and DNA damage due to microparticle exposure for gastrointestinal cells has been well studied in previous work.[7,57] Cell damage can be most acutely observed with PS-COOH particles, as there is a loss of intact lysosomes and late endosomes, indicated by the loss of LysoTracker deep red stain compared to PS (Fig. 3a).[7] All MP compositions and sizes are included in Fig. S4–S7.† The fold change in mean intensity for each of the red, blue, and green image channels is included to quantify changes that are difficult to see by eye (Fig. S7†). The particle compositions with the greatest fold-change in uptake, as measured by flow cytometry, were PS-COOH, PP, and PS-SA (Fig. 3b), indicating that mucus is a more effective barrier against these compositions. The fluorescence intensity plots for the "mucus" and "no mucus" groups are included in Fig. S8.† Due to the large range in the data, the fold change values are plotted in Fig. 3b and c. Low uptake was observed for PS-PEG, which is well known for being bioinert.[52]

Microscopy shows clear increase in particle uptake for smaller particles. We compared 500 nm and 40 nm PS-COOH particles (Fig. 3a). Cells without a mucus layer show diffuse green cytosolic fluorescence showing increased uptake of particles. The presence of mucus had the largest effect on the uptake fold change of 200 nm and 100 nm particles (Fig. 3c). All fold changes were statistically significant between no mucus and mucus groups (p-values < 0.0001). The presence of mucus did not greatly change the uptake of 500 nm particles likely due to the large particle size hindering uptake more generally and the smaller mucus mesh size. The smallest, 40 nm, particles had high absolute fluorescence with mucus present, leading to a low fold-change value and indicating that mucus is a less effective barrier for smaller particles (Fig. S8a and b†). The clear shift in fluorescent peaks due to particle uptake relative to the controls is shown in histograms for the flow cytometry data (Fig. S9a–l†). Overall, the microscopy and flow cytometry results highlight how the mucus barrier prevents cell damage and particle uptake.

3.3. Effects of MPs on the epithelial cell layer with and without the mucosal layer

To measure the role of mucus in protecting cells against MPs, we examined cytotoxicity and ROS production with an intact mucus layer and cells in which the mucus layer was delaminated and removed. Whereas some compositions may be easily taken up by cells with little effect, other plastics are highly cytotoxic, or result in oxidative stress, often an indication of inflammation.[31] Mucus offers clear protection with lower cytotoxicity for all compositions and sizes (Fig. 4). The control samples, for which no MPs are introduced, show a negligible increase in cytotoxicity indicating that the process of removing the mucus layer is not deadly to cells. Although the particles are ordered by increasing zeta potential, there is no correlation between surface charge and mortality with or without mucus present. The highest cytotoxicity levels are observed in cells exposed to PS-SA and PS-NH_2 functionalizations, while the lowest values are seen in PS-PEG. This may be due to SA and NH_2 binding to biotin or mucus readily, severely impacting cell processes, whereas PEG is known for being bioinert due to its affinity for water.[52,55,58] Cytotoxicity increases with decreasing size when a mucus layer is present with r = −0.95 (Fig. 4b). This trend is less obvious but still highly significant, without the mucus layer (r = −0.8). Mucus is less effective when the particles are smaller than the mesh size. The data highlights the critical role of gut mucus in preventing cytotoxicity for particles of various compositions particularly at sizes approaching or above the mesh size.

Mucus protection is also demonstrated by decreases in ROS production induced by any of the particle compositions and sizes (Fig. 4c and d). ROS production values were corrected based on the cytotoxicity levels of each particle type. ROS production was not significantly affected by the process of mucus removal. TBHP was used as a positive control, however, a low concentration was used such that the microparticles induced greater ROS levels. In contrast to cytotoxicity, ROS appears to show a trend with zeta potential. As surface charge increases, ROS production levels are higher, both when mucus is present (r = 0.66) and absent (r = 0.55). The most cytotoxic particles, PS-SA and PS-NH_2, also had the highest fold-change in ROS production. PS-PEG had low ROS production, in addition to low uptake seen in section 3.2. The ROS levels for PS-PEG are still comparable to other particles such as silica and PE. If PS-PEG is neglected from the statistical analysis due to its high zeta potential, the correlation coefficients for mucus and no mucus groups between ROS production and zeta potential increase to r = 0.81 and r = 0.73. ROS production strongly increases with decreasing particle size (mucus r = −0.80, no mucus r = −0.85) (Fig. 4d), although mucus clearly prevents ROS production in response to particles larger than or close to the mesh size and is much less effective against much smaller particles.

3.4. Mucus layer protection in an environmental context: MPs as vectors for other toxins

In addition to causing many negative health impacts, MPs also serve as a vector for other environmental toxins entering the body.[15] Drinking water and soil contains a cocktail of different MPs and pollutants.[17,59] We measured how the particle diffusivity, cell cytotoxicity, and ROS production vary when MPs are

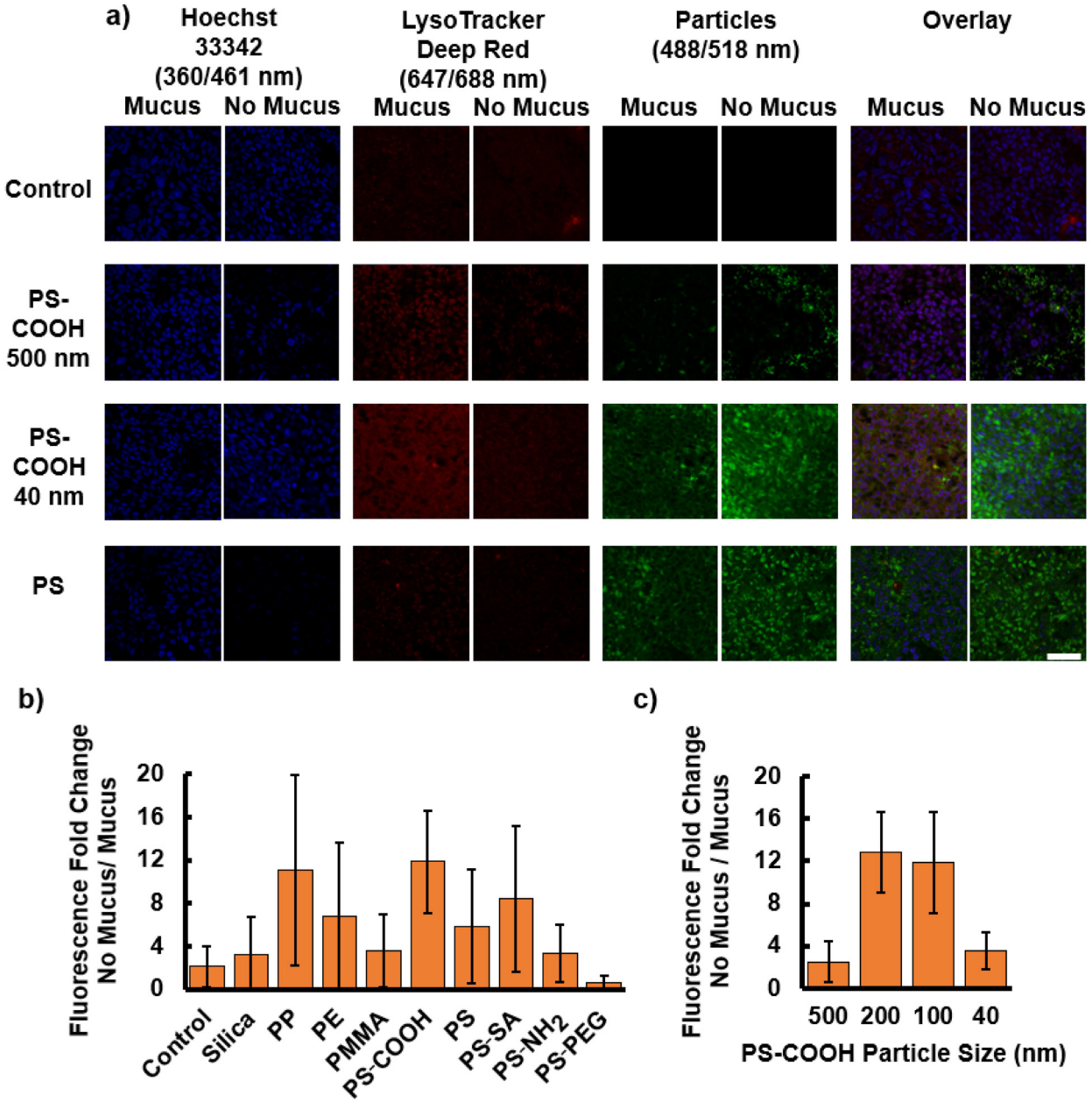

Fig. 3 Particle composition and size affect viability and uptake by HT-29-MTX cells. (a) HT-29-MTX cells, with intact mucus and with the mucus layer removed, treated with particles of various compositions and sizes, and stained with Hoechst 33342 and LysoTracker Deep Red. Overlay of all results is included with the scale bar = 100 μm for all images. All MP compositions and sizes are included in Fig. S4–S7.† Fig. S7† provides the percentage mean intensity for images for each channel to aid in visualizing small differences in intensity. (b) Particle uptake of microparticles, measured using the fold change in fluorescence, with varying compositions and (c) sizes with mucus and without mucus protecting cells. All fold changes were statistically significant between no mucus and mucus groups (p-values < 0.0001). Particles are listed in the order of increasing zeta potential.

combined with pollutants of concern to reflect the increased risk present in the environment. These tests were conducted based on previous MP concentrations used in previous *in vivo* mouse studies[45] and EPA limits for Cd, BHA, BPA, and DBP (Fig. 5).[16,18–20] Higher concentrations were also explored with cells co-exposed to particles and chemicals both at a concentration of 1 mg ml^{-1} to further highlight the differences between mucus and no mucus groups (Fig. S10†).

Chemicals decrease particle diffusivity for each toxin tested. First, the diffusivity of PS particles at 100 nm decreased significantly for each chemical (Fig. 5a). This may be due to an increase of dead cells and cellular debris that hindered particle migration. The change was most notable for BHA which also showed high cytotoxicity, particularly at the concentration of 1 mg ml^{-1} (Fig. 5b and S10b†). The addition of chemicals alters the expected diffusivity of MPs, indicating a need for

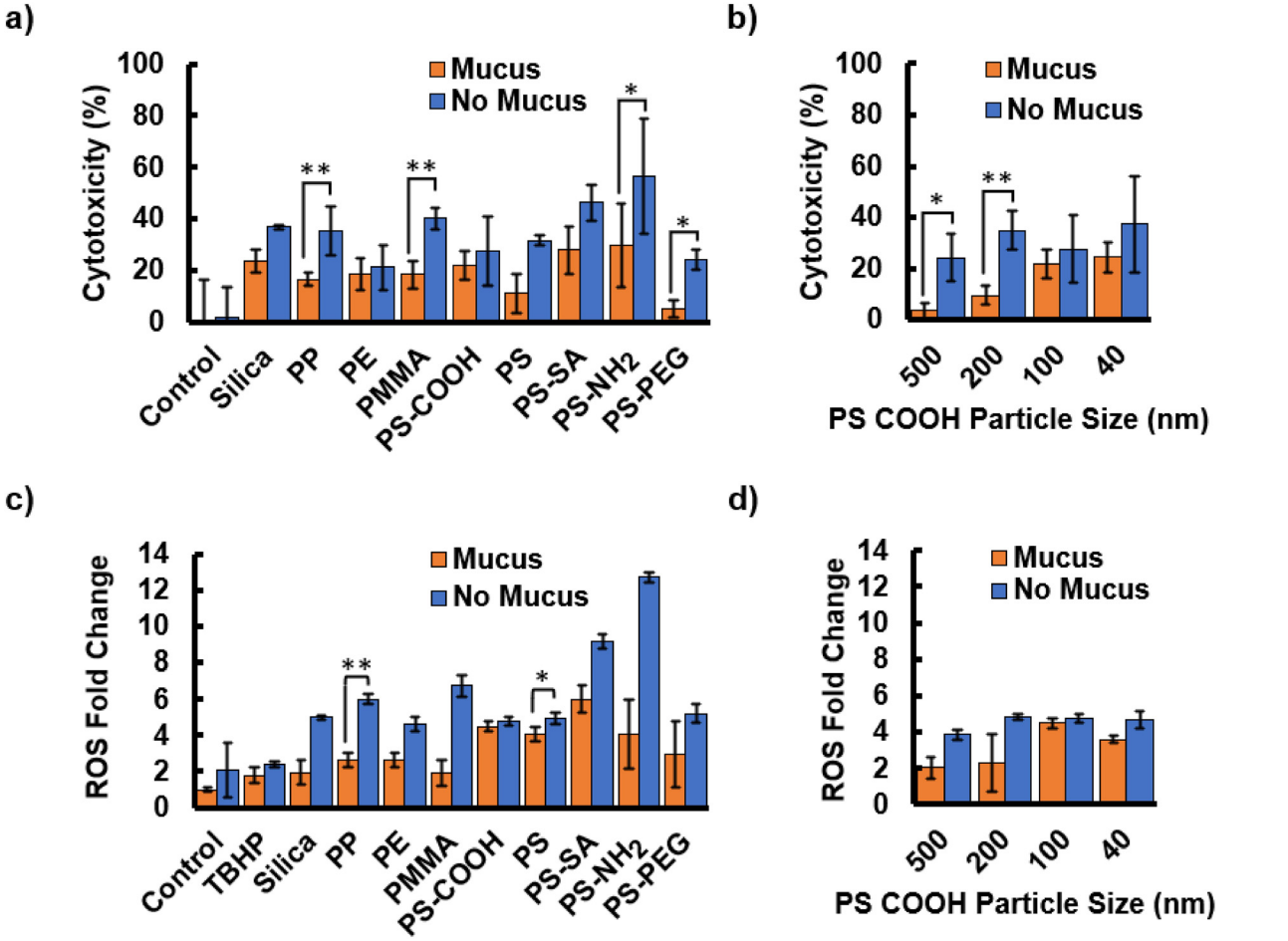

Fig. 4 The mucus layer protects cells from MP exposure-induced damage. (a) Cytotoxicity is measured for cells treated with MPs with different compositions, ordered by increasing zeta potential, and (b) sizes. (c) Reactive oxygen species fold change increases for MPs with different compositions and (d) sizes when the mucus layer is removed. Particles are listed in the order of increasing zeta potential.

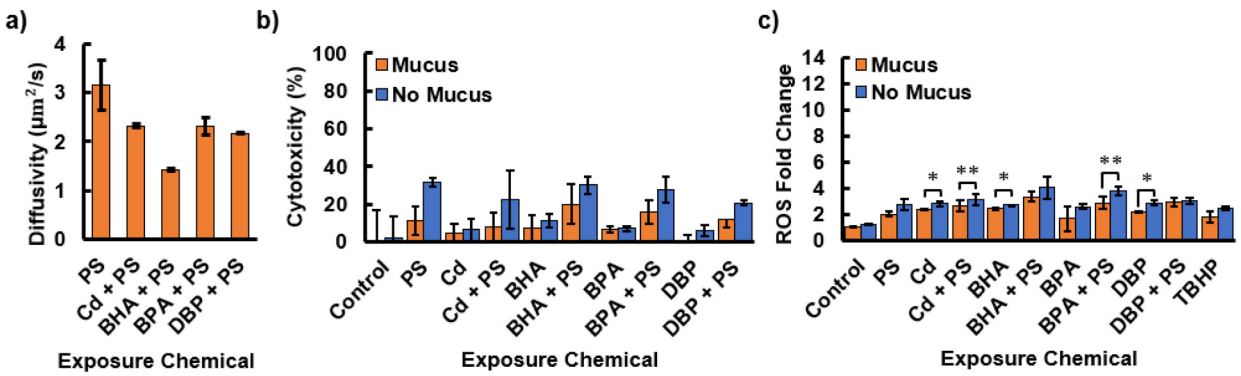

Fig. 5 The mucus layer protects against the combined effects of toxins and particles. (a) Diffusivity of PS particles in HT-29-MTX cell mucus following exposure to various environmental toxins at the EPA drinking water concentration limits. (b) Cytotoxicity with and without the mucus layer for environmental toxins alone and with PS particles. (c) Reactive oxygen species fold change for environmental pollutants with and without a mucus layer.

further study of how these changes in diffusivity affect cell responses, specifically cytotoxicity and ROS production.

In all cases, the mucus barrier appeared to play a role in protecting cells from cytotoxicity and ROS induction due to particles. For cytotoxicity, the combined chemical and particle treatment values were similar to the cytotoxicity of PS alone. The removal of mucus exacerbated cellular responses to the combined treatment, compared to MPs or chemicals in the

presence of mucus (Fig. 5b and c). The lack of a significant difference in Cd and Cd with particles is likely due to the close environmental control on heavy metals leading to a very low EPA limit. At the EPA concentrations the chemicals do not appear to greatly increase the cytotoxicity beyond that of solely MPs. ROS production for all cells treated with chemicals was significantly increased compared to the no chemical control groups except for BPA with mucus present. Chemicals also increased the ROS production in the presence of particles compared to particles alone. At chemical concentrations above the EPA limits (Fig. S10†), the effects of combined particles and pollutants is much higher than each toxin alone. These tests support the need for public health regulation specifically addressing the combined effects of environmental toxins and MPs.

4. Conclusions

We examined how MP migration in human intestinal mucus varies based on particle composition, surface functionalization, and size. Mucus proved most effective at blocking highly charged and larger particles with diameters close to or larger than the mucus mesh size. This study also examined the barrier function of mucus through investigating cell responses, including uptake, cytotoxicity, and ROS production, in the presence and absence of the mucus layer. Results highlight the role of mucus as a protective barrier for particle transport, preventing cytotoxicity, ROS production, and uptake for all compositions and sizes. Notable particle groups were PS-SA and PS-NH_2 which induced high ROS production and cytotoxicity likely due to biotin binding and other interactions with mucus. The most abundant MPs in the environment due to single-use plastics, PP, PE, and PS, had high diffusivity values but were shown to induce only moderate levels of cytotoxicity and ROS production. However, the cellular response was much higher when cells were co-exposed to PS and high concentrations of other environmental toxins. PE and PS are often used in food packaging and disposable water bottles and are likely to encounter chemicals used as food preservatives, such as BHA, and plastic additives, including BPA and DBP. The response to combined MPs and chemicals highlights the need for public health regulations of chemicals that can use MPs as vectors to migrate throughout the body as higher cytotoxicity and ROS production were observed when chemicals surpassed EPA limits. We demonstrated that adding chemicals alters MP diffusivity in mucus and co-exposure of particles with environmental chemicals can exacerbate cell responses compared to chemicals of plastics alone.

Our work identifies the risk certain MPs have for individuals with reduced mucus barrier function, however additional studies are required to address the limitations of this study through further exploration of the effects of mucus composition, an even broader array of surface functionalizations, and to develop better microplastic detection methods. Additional properties such as shape and hydrophobicity also merit further study. Various inflammation associated gastrointestinal diseases alter the composition of mucus itself and may change how particles migrate and interact with the mucus barrier. For example, patients with Crohn's disease have a lower mesh size for mucus which may assist in lower particle migration but also have lower fluid in the mucus and incomplete glycoproteins which decreases mucus shedding and may alter particle diffusion.[60,61] Leveraging a microfluidic platform in combination with our mucus layer may further improve our model. Understanding how a broader array of surface functionalizations, including antibody and drug functionalizations interact with different mucus compositions would also help in developing treatments for these conditions.[62] This study was limited to "virgin" microplastics. Future work is also needed to address how microplastics that have interacted with other pollutants, beyond heavy metals, affect the intestinal epithelia. Lastly, current detection methods are often limited to ~100 nm sized particles. Improved techniques are required for bioremediation of MPs and to identify health risks.[5] These future research directions will advance both medical care and environmental stewardship.

Author contributions

The manuscript was written through contributions of all authors. All authors have given approval to the final version of the manuscript. Conceptualization, I. L. B., M. N. S.; data curation, E. W. v. W., M. R.; Experimental Design, E. W. v. W., S. A.; formal analysis, E. W. v. W.; writing-original draft preparation, E. W. v. W.; writing – review and editing, I. L. B., M. N. S.; visualization, E. W. v. W.; supervision, I. L. B., M. N. S.; project administration, I. L. B.; funding acquisition, I. L. B., M. N. S.

Data availability

Data for this article are available at BOX at [**https://cornell.app.box.com/s/xptgb31qvpknul2z5w2dpaqxl6bcdndw**].

Conflicts of interest

There are no conflicts to declare.

Acknowledgements

NSERC PGS-D scholarship (E. W. v. W., award number PGS D - 577273 - 2023). This work was performed in part at the Engineered Living Materials Institute and Cornell NanoScale Facility, a member of the National Nanotechnology Coordinated Infrastructure (NNCI), which is supported by the National Science Foundation (Grant NNCI69 2025233). Herbert W. Hoover Foundation (I. L. B.).

References

1 Y. Li, L. Tao, Q. Wang, F. Wang, G. Li and M. Song, *Environ. Health*, 2023, **1**, 249–257.
2 N. O. and A. A. US Department of Commerce, What are microplastics?, **https://oceanservice.noaa.gov/facts/microplastics.html**, (accessed 18 June 2024).
3 Q. Zhang, E. G. Xu, J. Li, Q. Chen, L. Ma, E. Y. Zeng and H. Shi, *Environ. Sci. Technol.*, 2020, **54**, 3740–3751.
4 K. D. Cox, G. A. Covernton, H. L. Davies, J. F. Dower, F. Juanes and S. E. Dudas, *Environ. Sci. Technol.*, 2019, **53**, 7068–7074.
5 N. Qian, X. Gao, X. Lang, H. Deng, T. M. Bratu, Q. Chen, P. Stapleton, B. Yan and W. Min, *Proc. Natl. Acad. Sci. U. S. A.*, 2024, **121**, e2300582121.
6 R. A. Cone, *Adv. Drug Delivery Rev.*, 2009, **61**, 75–85.
7 G. Visalli, A. Facciolà, M. Pruiti Ciarello, G. De Marco, M. Maisano and A. Di Pietro, *Int. J. Environ. Res. Public Health*, 2021, **18**, 5833.
8 L. Lu, Z. Wan, T. Luo, Z. Fu and Y. Jin, *Sci. Total Environ.*, 2018, **631–632**, 449–458.
9 Y. Jin, L. Lu, W. Tu, T. Luo and Z. Fu, *Sci. Total Environ.*, 2019, **649**, 308–317.
10 B. Li, Y. Ding, X. Cheng, D. Sheng, Z. Xu, Q. Rong, Y. Wu, H. Zhao, X. Ji and Y. Zhang, *Chemosphere*, 2020, **244**, 125492.
11 Y. Chen, A. M. Williams, E. B. Gordon, S. E. Rudolph, B. N. Longo, G. Li and D. L. Kaplan, *Nanomedicine*, 2023, **50**, 102680.
12 Y.-F. Yang, C.-Y. Chen, T.-H. Lu and C.-M. Liao, *J. Hazard. Mater.*, 2019, **366**, 703–713.
13 M. M. Garcia, A. S. Romero, S. D. Merkley, J. L. Meyer-Hagen, C. Forbes, E. E. Hayek, D. P. Sciezka, R. Templeton, J. Gonzalez-Estrella, Y. Jin, H. Gu, A. Benavidez, R. P. Hunter, S. Lucas, G. Herbert, K. J. Kim, J. Y. Cui, R. R. Gullapalli, J. G. In, M. J. Campen and E. F. Castillo, *Environ. Health Perspect.*, 2024, **132**, 047005.
14 C. E. Sofield, R. S. Anderton and A. M. Gorecki, *Curr. Issues Mol. Biol.*, 2024, **46**, 4186–4202.
15 W. Huang, B. Song, J. Liang, Q. Niu, G. Zeng, M. Shen, J. Deng, Y. Luo, X. Wen and Y. Zhang, *J. Hazard. Mater.*, 2021, **405**, 124187.
16 Cadmium Public Health Statement ATSDR, **https://wwwn.cdc.gov/TSP/PHS/PHS.aspx?phsid=46&toxid=15**, (accessed 12 July 2024).
17 E. Tumwesigye, C. F. Nnadozie, F. C. Akamagwuna, X. S. Noundou, G. W. Nyakairu and O. N. Odume, *Environ. Pollut.*, 2023, **330**, 121829.
18 Bisphenol A Action Plan, U.S. Environmental Protection Agency, 2010, **http://www.regulations.gov/#!documentDetail;D=EPA-HQ-OPPT-2010-0348-0002**, (accessed 18 June 2024).
19 P. Wagner, *Inert Reassessment Document for Butylated Hydroxyanisole*, U.S. Environmental Protection Agency, 2015.
20 S. Schatzow, *Ambient Water Quality Criteria for Phthalate Esters*, U.S. Environmental Protection Agency, Washington, D.C., 1980.
21 J. McCright, A. Sinha and K. Maisel, *Cell. Mol. Bioeng.g*, 2022, **15**, 479–491.
22 Y. Bhattarai, S. Jie, D. R. Linden, S. Ghatak, R. A. T. Mars, B. B. Williams, M. Pu, J. L. Sonnenburg, M. A. Fischbach, G. Farrugia, L. Sha and P. C. Kashyap, *iScience*, 2020, **23**(12), 101798.
23 S. S. Datta, A. P. Steinberg and R. F. Ismagilov, *Proc. Natl. Acad. Sci. U. S. A.*, 2016, **113**, 7041–7046.
24 J. A. Grondin, Y. H. Kwon, P. M. Far, S. Haq and W. I. Khan, *Front. Immunol.*, 2020, **11**, 2054.
25 L. Zhao, S. L. Arias, W. Zipfel, I. L. Brito and J. Yeo, *Int. J. Biol. Macromol.*, 2024, **267**, 131434.
26 A. E. Dorofeyev, I. V. Vasilenko, O. A. Rassokhina and R. B. Kondratiuk, *Gastroenterol. Res. Pract.*, 2013, **2013**, 431231.
27 M. S. Desai, A. M. Seekatz, N. M. Koropatkin, N. Kamada, C. A. Hickey, M. Wolter, N. A. Pudlo, S. Kitamoto, N. Terrapon, A. Muller, V. B. Young, B. Henrissat, P. Wilmes, T. S. Stappenbeck, G. Núñez and E. C. Martens, *Cell*, 2016, **167**, 1339–1353.
28 A. Tamargo, N. Molinero, J. J. Reinosa, V. Alcolea-Rodriguez, R. Portela, M. A. Bañares, J. F. Fernández and M. V. Moreno-Arribas, *Sci. Rep.*, 2022, **12**, 528.
29 P. Krasucka, A. Bogusz, E. Baranowska-Wójcik, B. Czech, D. Szwajgier, M. Rek, Y. S. Ok and P. Oleszczuk, *Sci. Total Environ.*, 2022, **843**, 157108.
30 S. Li, Y. Ma, J. Cui, F. Caruso and Y. Ju, *Chem. Commun.*, 2024, **60**, 2591–2604.
31 G. F. Schirinzi, I. Pérez-Pomeda, J. Sanchís, C. Rossini, M. Farré and D. Barceló, *Environ. Res.*, 2017, **159**, 579–587.
32 E. Brynzak-Schreiber, E. Schögl, C. Bapp, K. Cseh, V. Kopatz, M. A. Jakupec, A. Weber, T. Lange, J. L. Toca-Herrera, G. del Favero, W. Wadsak, L. Kenner and V. Pichler, *Chemosphere*, 2024, **353**, 141463.
33 M. Hesler, L. Aengenheister, B. Ellinger, R. Drexel, S. Straskraba, C. Jost, S. Wagner, F. Meier, H. von Briesen, C. Büchel, P. Wick, T. Buerki-Thurnherr and Y. Kohl, *Toxicol. in Vitro*, 2019, **61**, 104610.
34 J. Hwang, D. Choi, S. Han, S. Y. Jung, J. Choi and J. Hong, *Sci. Rep.*, 2020, **10**, 7391.
35 V. Stock, L. Böhmert, E. Lisicki, R. Block, J. Cara-Carmona, L. K. Pack, R. Selb, D. Lichtenstein, L. Voss, C. J. Henderson, E. Zabinsky, H. Sieg, A. Braeuning and A. Lampen, *Arch. Toxicol.*, 2019, **93**, 1817–1833.
36 D. Ke, J. Zheng, X. Liu, X. Xu, L. Zhao, Y. Gu, R. Yang, S. Liu, S. Yang, J. Du, B. Chen, G. He and R. Dong, *EBioMedicine*, 2023, **97**, 104828.
37 P. Schwabl, S. Köppel, P. Königshofer, T. Bucsics, M. Trauner, T. Reiberger and B. Liebmann, *Ann. Intern. Med.*, 2019, **171**, 453–457.
38 D. Pavičić-Hamer, I. Kovačić, T. Sović, M. Marelja and D. M. Lyons, *Fishes*, 2022, **7**, 307.
39 CFR - Code of Federal Regulations Title 21, **https://www.accessdata.fda.gov/scripts/cdrh/cfdocs/cfcfr/CFRSearch.cfm?fr=172.480**, (accessed 16 December 2024).

40 Y. Chenyakin, D. A. Ullmann, E. Evoy, L. Renbaum-Wolff, S. Kamal and A. K. Bertram, *Atmos. Chem. Phys.*, 2017, **17**, 2423–2435.
41 M. Abdulkarim, N. Agulló, B. Cattoz, P. Griffiths, A. Bernkop-Schnürch, S. G. Borros and M. Gumbleton, *Eur. J. Pharm. Biopharm.*, 2015, **97**, 230–238.
42 L. D. Li, T. Crouzier, A. Sarkar, L. Dunphy, J. Han and K. Ribbeck, *Biophys. J.*, 2013, **105**, 1357–1365.
43 R. M. Shobar, S. Velineni, A. Keshavarzian, G. Swanson, M. T. DeMeo, J. E. Melson, J. Losurdo, P. A. Engen, Y. Sun, L. Koenig and E. A. Mutlu, *Clin. Transl. Gastroenterol.*, 2016, **7**, e143.
44 J. Celli, B. Turner, N. Afdhal, R. Ewoldt, G. McKinley, R. Bansil and S. Erramilli, *Biomacromolecules*, 2007, **8**, 1580–1586.
45 R. Jia, J. Han, X. Liu, K. Li, W. Lai, L. Bian, J. Yan and Z. Xi, *Toxics*, 2023, **11**, 127.
46 J.-Y. Tinevez, N. Perry, J. Schindelin, G. M. Hoopes, G. D. Reynolds, E. Laplantine, S. Y. Bednarek, S. L. Shorte and K. W. Eliceiri, *Methods*, 2017, **115**, 80–90.
47 X.-D. Bu, N. Li, X.-Q. Tian, L. Li, J.-S. Wang, X.-J. Yu and P.-L. Huang, *World J. Gastroenterol.*, 2010, **16**, 4089.
48 P. J. Moncure, Z. C. Simon, J. E. Millstone and J. E. Laaser, *J. Phys. Chem. B*, 2022, **126**, 4132–4142.
49 L.-H. Cai, S. Panyukov and M. Rubinstein, *Macromolecules*, 2015, **48**, 847–862.
50 M. E. V. Johansson, J. M. H. Larsson and G. C. Hansson, *Proc. Natl. Acad. Sci. U. S. A.*, 2011, **108**, 4659–4665.
51 E. Y. Chen, D. Daley, Y.-C. Wang, M. Garnica, C.-S. Chen and W.-C. Chin, *Sci. Rep.*, 2012, **2**, 211.
52 Q. Xu, L. M. Ensign, N. J. Boylan, A. Schön, X. Gong, J.-C. Yang, N. W. Lamb, S. Cai, T. Yu, E. Freire and J. Hanes, *ACS Nano*, 2015, **9**, 9217–9227.
53 S. L. McGill and H. D. C. Smyth, *Mol. Pharm.*, 2010, **7**, 2280–2288.
54 S. Sabui, R. Kapadia, A. Ghosal, M. Schneider, N. W. G. Lambrecht and H. M. Said, *Am. J. Physiol.: Cell Physiol.*, 2018, **315**, C73–C79.
55 J. C. Yang, J. P. Jacobs, M. Hwang, S. Sabui, F. Liang, H. M. Said and J. Skupsky, *Nutrients*, 2023, **15**, 264.
56 A. Cobarrubia, J. Tall, A. Crispin-Smith and A. Luque, *Front. Phys.*, 2021, **9**, 594306.
57 P. Møller and M. Roursgaard, *Mutat. Res., Rev. Mutat. Res.*, 2024, **793**, 108491.
58 Y.-Y. Wang, S. K. Lai, C. So, C. Schneider, R. Cone and J. Hanes, *PLoS One*, 2011, **6**, e21547.
59 M. Sajjad, Q. Huang, S. Khan, M. A. Khan, Y. Liu, J. Wang, F. Lian, Q. Wang and G. Guo, *Environ. Technol. Innovation*, 2022, **27**, 102408.
60 C. Kramer, H. Rulff, J. F. Ziegler, N. Alzain, A. Addante, A. Kuppe, S. Timm, P. Schrade, P. Bischoff, R. Glauben, J. Dürr, M. Ochs, M. A. Mall, M. Gradzielski and B. Siegmund, *bioRxiv*, 2024, preprint, DOI: **10.1101/2024.01.03.574052**.
61 Y. Kang, H. Park, B.-H. Choe and B. Kang, *Front. Med.*, 2022, **9**, 848344.
62 Y. Kumar, A. S. K. Sinha, K. D. P. Nigam, D. Dwivedi and J. S. Sangwai, *Nanoscale*, 2023, **15**, 6075–6104.